Available online at www.sciencedirect.com

ScienceDirect

Ceramics International 40 (2014) 1–9

CERAMICS INTERNATIONAL

www.elsevier.com/locate/ceramint

Review paper

Effect of soaking time on the photoluminescence properties of cerium oxide nanoparticles

R.C. Deus[a,1], C.R. Foschini[c,2], B. Spitova[d,3], F. Moura[b,4], E. Longo[c,2], A.Z. Simões[a,b,*,4]

[a]*Universidade Estadual Paulista – Unesp – Faculdade de Engenharia de Guaratingueta, Avenue Doutor Ariberto Pereira da Cunha 333, Bairro Pedregulho, P.O. Box 355, 12516-410 Guaratinguetá, São Paulo, Brazil*

[b]*Universidade Federal de Itajubá – Unifei – Campus Itabira, Rua São Paulo 377, Bairro Amazonas, P.O. Box 355, 35900-37 Itabira, Minas Gerais, Brazil*

[c]*Laboratório Interdisciplinar em Cerâmica, Instituto de Química, Universidade Estadual Paulista, P.O. Box 355, 14801-907 Araraquara, São Paulo, Brazil*

[d]*VSB-Technical University of Ostrava, Faculty of Metallurgy and Materials Engineering, 17. listopadu 15/2172, 708 33 Ostrava-Poruba, Czech Republic*

Received 21 February 2013; received in revised form 12 June 2013; accepted 13 June 2013
Available online 27 June 2013

Abstract

The structural and photoluminescence properties at room temperature of CeO_2 nanoparticles synthesized by a microwave-assisted hydrothermal method (MAH) under different soaking times on KOH mineralizer added to a cerium ammonium nitrate aqueous solution were undertaken. X-ray diffraction (XRD), Fourier transform infrared (FT-IR), Fourier transform Raman (FT-Raman) and photoluminescence (PL) measurements were employed. XRD revealed that the nanoparticles are free of secondary phases and crystallize in the cubic structure. The UV/vis absorption spectroscopy suggested the presence of intermediate energy levels in the band gap of structurally ordered powders. The most intense PL emission was obtained for nanoparticles which represent a lower particle size.

Keywords: A. Ceramics; B. Chemical syntheses; B. Powder metallurgy; C. X-ray diffraction

Contents

1. Introduction

Order–disorder effects are the keys to many unsolved structural problems and unexplained structure-related properties in solid materials. In particular, structural order–disorder is always present in real materials and may play an important role in technological applications by altering their electronic and optical properties. Therefore, physical principles that govern the structural state of a given perovskite and how that state may change have long been the subject of investigation and debate. Ceria (CeO_2) has been considered an important

*Corresponding author at: Universidade Estadual Paulista – Unesp – Faculdade de Engenharia de Guaratingueta, Avenue Doutor Ariberto Pereira da Cunha 333, Bairro Pedregulho, P.O. Box 355, 12516-410 Guaratinguetá, São Paulo, Brazil. Tel.: +55 12 3123 2765; fax: +55 12 3123 2800.
E-mail address: alezipo@yahoo.com (A.Z. Simões).
[1]Tel.: +55 12 3123-2765; fax: +55 12 3123-2800.
[2]Tel.: +55 16 3301-6643; fax: +55 16 3301-6692.
[3]Tel.: +420 597 324 230; fax: +420 596 918 507.
[4]Tel.: +55 31 3834-6472; fax: +55 31 3834-6136.

0272-8842/$ - see front matter © 2013 Elsevier Ltd and Techna Group S.r.l. All rights reserved.
http://dx.doi.org/10.1016/j.ceramint.2013.06.043

nanomaterial for applications in catalysts [1,2], fuel cells [3], ultraviolet absorbers [4], hydrogen storage materials [5], oxygen sensors [6], optical devices [7], polishing materials [8], and for which the use of nanocrystalline powders is an important factor. Several methods have been developed to prepare ultrafine $Ce_{1-x}Gd_xO_2$ powder, including hydrothermal [10], precipitation (for oxalate [11], carbonate [12,13], peroxide [9], and hydroxide [14]), polymeric precursor [15,16], complexion with citric acid [15], the flow method [17], organometallic decomposition [18] and the microwave-assisted heating technique [19–21].

Among the various methods, the hydrothermal crystallization is an interesting process to directly prepare pure fine oxide powders with reduced contamination and low synthesis temperature. The conventional-hydrothermal method requires longer soaking times at a low temperature (below 200 °C) to obtain the ceria powders. For this reason, the introduction of microwave heating to the conventional-hydrothermal method is advantageous for the synthesis of various ceramic powders because microwave heating permits a reduction of processing time and energy cost. Likewise, particles with desired size and shape can be produced if parameters such as solution pH, reaction temperature, reaction time, solute concentration and the type of solvent are carefully monitored [22]. A modification of the hydrothermal method developed by Komarneni et al. [23–25] involves the introduction of microwaves during the hydrothermal synthesis to increase the kinetics of crystallization by one to two orders of magnitude compared to the conventional hydrothermal. The microwave-assisted hydrothermal (MAH) method shows advantages such as rapidity, convenience and cost-effectiveness. Ceria systems with nanosized particles were successfully synthesized by the MAH method utilizing a relatively low temperature and short reaction time [26]. Here, the authors describe the formation conditions of ceria via the MAH method reported in detail, and the advantages of microwave irradiation introduced.

As we know, there are few works describing MAH route for the synthesis of pure CeO_2 nanoparticles. Gao et al. [27] reported for the first time the preparation of ceria nanoparticles (1.6 nm) and nanorods (20 nm) under microwave-assisted conditions. Corradi et al. [28] also reported the synthesis of cubic CeO_2 crystals (5.7 nm) under microwave-assisted hydrothermal route around 194 °C for only 5 min. No calcination process or surfactant was required. The MAH method is getting very attractive in all areas of synthetic chemistry because it can boost some advantages over other synthetic methods [29]. This method has been extensively used in organic synthesis [30–32] and more recently this technique has also been widely applied to prepare inorganic nanostructured materials [33–36] with a wide range of applications [37–39]. In particular, Bilecka and Niederberger have reported the versatility of the method for the synthesis of nanoparticles [40], while Baghbanzadeh et al. [41] have presented a complete review on the subject. Silva et al. [42] prepared $SrTi_{1-x}Fe_xO_3$ nanocubes by means of a microwave-assisted hydrothermal (MAH) method at 140 °C. According to high-resolution transmission electron microscopy (HRTEM) results, these nanocubes are formed by a self-assembly process of small primary nanocrystals. In the another paper of the group [43], $BaZrO_3$ (BZO) nanoparticles were nucleated, grown and subsequently self-assembled into a 3D decaoctahedronal architecture via a microwave-assisted hydrothermal (MAH) method. A theoretical model, based on the presence of uncoordinated bonds and/or charge distribution in the distorted constituent clusters (ZrO_6) and (BaO_{12}) of the material, can be related to the change in both surface and internal defects during crystal growth. $BaZrO_3$ microcrystals were also obtained using the microwave assisted hydrothermal method (MAH) at 140 °C for 40 min [44]. The growth mechanism for the formation of $BaZrO_3$ with decaoctahedron-shape was analyzed in detail, and the nature of the mechanism follows a non-classical growth process involving mesoscale self-assembly of nanoparticles.

The PL emission is considered to be closely related to the crystal structure and their corresponding distorted metal–oxygen polyhedra. Among the properties of pure or doped cerium oxide nanoparticles, photoluminescence has been the object of several publications [45–50] but these may appear as not very conclusive as some experimental facts were not definitely explained. For example, even the attribution of the most intense peak at 400 nm to Ce_6O_{11} clusters firstly proposed by Djuricic and Pickering [51], was considered hypothetical by the authors themselves. Comparisons of results from different studies are complicated due to the fact that different syntheses produce particles with different surfaces or bulk defects, oxygen vacancies and ratio of reduced Ce^{3+}. The point is 4 or 5 bands may appear in a relatively narrow region around 400 nm and their respective attribution is not clear, to our knowledge.

On this basis, systematic experiments may be useful to extract reliable information from photoluminescence spectra. The aim of the present work was to compare photoluminescence spectra of CeO_2 nanoparticles annealed at different soaking times obtained in the same experimental conditions focusing on links between the structure and the photoluminescent behavior of CeO_2 nanoparticles through a simple and fast microwave-assisted hydrothermal (MAH) method.

2. Experimental procedure

CeO_2 nanoparticles were synthesized by a hydrothermal microwave route. Cerium(IV) ammonium nitrate (5×10^{-3} mol L^{-1} $Ce(NH_4)_2(NO_3)_6$, 99.9% purity) was dissolved in 80 ml of deionized water under constant stirring for 15 min at room temperature. Subsequently, 1 ml of 2 M KOH (p.a, Merck) was slowly added in the solution until the pH 10 was reached. The resulted solution was transferred into a sealed Teflon autoclave and placed in a hydrothermal microwave (2.45 GHz, maximum power of 800 W). The reactional system was heat treated at 100 °C for different soaking times (1, 2, 4 and 8 min) with a heating rate fixed at 10 °C/min. The pressure in the sealed autoclave was stabilized at 1.2 atm. The autoclave was cooled to the room temperature naturally. CeO_2 nanoparticles were collected and washed with acetone several

times and then dried at 80 °C in an oven. The obtained nanoparticles were characterized by X-ray powder diffraction (XRD) using a (Rigaku-DMax/2500PC, Japan) with Cu-Kα radiation ($\lambda = 1.5406$ Å) in the 2θ range from 20° to 75° with 0.2 deg/min. The crystallite size (d) of CeO_2 was calculated using Scherrer equation $d = k\lambda/\beta \cos\theta$, where k is constant, λ is the wavelength of X-rays and β is the full width at half maximum (FWHM) for (1 1 1) reflection measured from slow scan where θ is the diffraction angle of the main peak. Raman spectra were collected (Bruker RFS-100/S Raman spectrometer with Fourier transform). A 1064 nm YAG laser was used as the excitation source, and its power was kept at 150 mW. The FT-IR spectra were recorded with a Bruker Equinox-55 instrument. Infrared spectroscopy was used for monitoring the structural changes occurring during the synthesis process with the KBr pellet technique. The morphology of as-prepared samples was observed using a high resolution field-emission gun scanning electron microscopy FEG-SEM (Supra 35-VP, Carl Zeiss, Germany). Specimens for TEM were obtained by drying droplets of the as-prepared samples from an ethanolic dispersion which had been sonicated for 5 min onto 300 mesh Cu grids. TEM images and SAD patterns were then obtained at an accelerating voltage of 200 kV by a Philips model CM 200 instrument. All measurements were done at the room temperature. Ultraviolet–visible (UV–vis) spectroscopy for the optical absorbance spectra of CeO_2 powders was taken using a Cary 5G equipment. PL properties were measured with a Thermal Jarrel-Ash Monospec 27 monochromator and a Hamamatsu R446 photomultiplier. The excitation source was 350.7 nm wavelength of a krypton ion laser (Coherent Innova) keeping their power at 200 mW. All measurements were performed at the room temperature.

3. Results and discussion

The powder XRD patterns of the as-prepared ceria nanoparticles showed the same crystalline structure for all the synthesis conditions used (Fig. 1). All of the peaks can be well-indexed to a pure cubic structure of CeO_2 (space group: $Fm3m$) with lattice constant $a = 5.411$ Å, which is in good agreement with the JCPDS file for CeO_2 (JCPDS 34-394). It is worth noting that the overwhelmingly intensive diffraction peak is located at $2\theta = 28.660°$, which is from the [1 1 1] lattice plane of fcc CeO_2. No peak of any other phase was detected. The broadening of the peaks indicates that the crystallite sizes are small (4–9 nm), following the literature [52]. The average crystallite sizes calculated by Debye Scherrer are around 5.80, 7.03, 8.80 and 11.50 nm at soaking times of 1, 2, 4 and 8 min, respectively. It is obvious that the soaking time changes the CeO_2 crystal growth. As the average diffusion distance for the diffusing solute is short and the concentration gradient is steep in concentrated solutions, much diffusing material passes per unit time through an unit area. A clear evidence that CeO_2 is formed instead $Ce(OH)_x$ comes from the fact that nitrate salts of ceria were preferably used since these salts were easily dissociable in few milliliters of water and the friable mass formed (Ce^{4+}) after treating with acid, reacted spontaneously

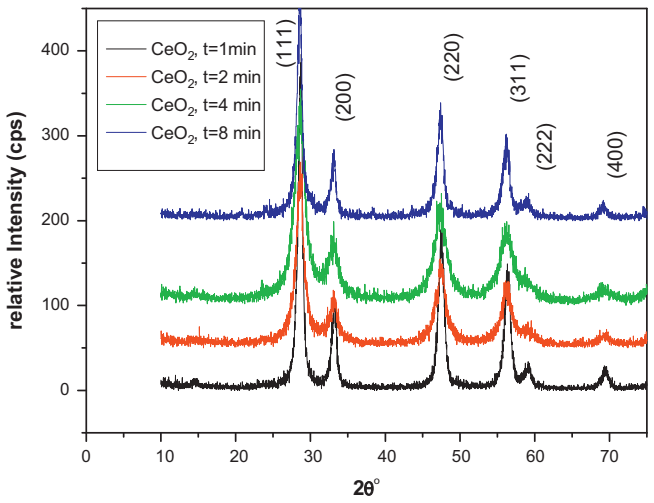

Fig. 1. X-ray diffraction pattern of CeO_2 nanoparticles synthesized at 100 °C by the MAH method under different soaking times: (a) 1 min; (b) 2 min; (c) 4 min and (d) 8 min.

with the mineralizer to produce a highly exothermic reaction. When cerium nitrate is used as the precursor salt and reacted with an acid to dissolve it, the Ce^{3+} ion is oxidized to Ce^{4+} ion and then acidic mass reacts exothermically with the mineralizer. It forms a by-product salt (KNO_3) that surrounds the hydroxide product. In the oxidizing atmosphere, dehydration occurs, converting the hydroxide intermediate to oxide. In the MAH methods, the conversion to oxide is more rapid due to the effect of energetic radiations assisting the transformation to CeO_2 instead $Ce(OH)_x$.

Fig. 2 shows FTIR spectral features of CeO_2 samples at a soaking time of 8 min. Strong intense bands at 3435, 2358, 1589 cm^{-1} and below 700 cm^{-1} were observed. The intense bands at 3435 and 1589 cm^{-1} correspond to the ν (O–H) mode of (H-bonded) water molecules and δ (OH), respectively. Residual water and hydroxy group are usually detected in the as prepared ceria samples regardless of synthesis method used [53] and further heat treatment is necessary for their elimination. The FTIR spectrum of the ceria also exhibits a strong broad band below 700 cm^{-1} which is due to the δ (Ce–O–C) mode. Specifically, the strong absorptive peaks at 400–600 cm^{-1} were attributed to the Ce–O stretching and bending vibration, being characteristics of the tetrahedral CeO_4 groups in the compounds. The hydroxylation and deprotonation of metal ions can be accelerated by raising the solution temperature or pressure [54]. A sharp band at 1055 cm^{-1} was attributed to the vibrations associated with the incoordination of the adsorbed NO_3^{1-} ions [55]. Band in the 2358 cm^{-1} region was attributed to the stretching frequency of the acetone group. That suggests that the acetone group was chemically bonded to the surface of the ceria nanocrystals. This is probably the result of reactions forming chemical bonds between the nanocrystal surface and the organic-ligand molecule in the unique reaction conditions of supercritical water, which are essential for the perfect dispersion of nanocrystals in organic solvents and for the arrangement of individual nanocrystals into superlattices and new studies should be

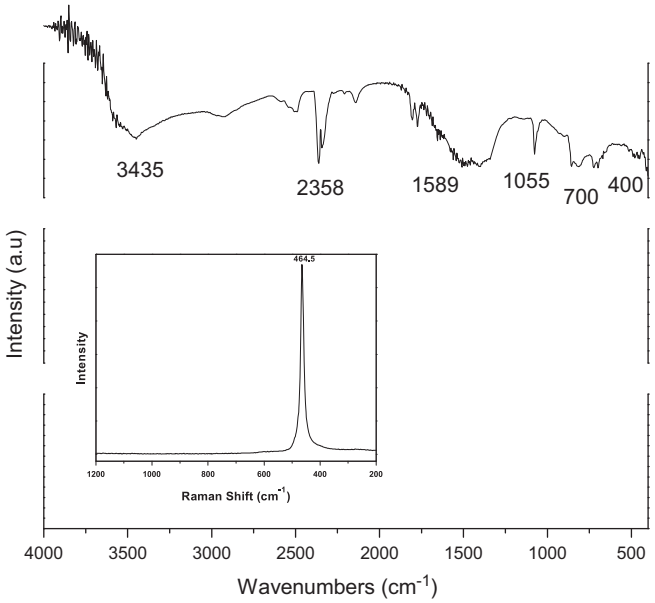

Fig. 2. FT-IR spectra of CeO_2 nanoparticles synthesized at 100 °C for 8 min by the MAH method. Inset of Fig. 2 shows Raman spectra of CeO_2 nanoparticles synthesized at 100 °C for 8 minutes by the MAH method under a soaking time of 8 min.

performed to avoid its presence. The crystallized nanoparticle was found to have OH^- ions due to the alkali used in the present reaction conditions. Following the literature, hydrolysis refers to those reactions of metallic ions with water that liberate protons and produce hydroxide or oxide solids. Ce^{4+} ions, which have a low basicity and high charge, undergo strong hydration. Firstly, Ce^{4+} ions are hydrolyzed and form complexes with water molecules or OH^- to give $[Ce(OH)_x(H_2O)_y]^{(4-x)+}$, where $x+y$ is the coordination number of Ce^{4+}. Further polymerization is likely, and both species can serve as the precursors for the final ceria nanoparticles. In an aqueous solution, H_2O being a polar molecule, tends to take protons away from coordinated hydroxide, leading to the formation of $CeO_2 \cdot nH_2O$. This process can be described by the following equations [56]:

$$Ce^{4+} + xOH + yH_2O \rightarrow [Ce(OH)_x(H_2O)_y]^{(4-x)+} \quad (1)$$

$$[Ce(OH)_x(H_2O)_y]^{(4-x)+} + H_2O \rightarrow CeO_2 \cdot nH_2O + nH_2O + H_3O^+ \quad (2)$$

The inset in Fig. 2 confirms the formation of pure ceria by FT-Raman spectrum. Cubic fluorite structure-metal dioxides have a single Raman mode at 464.5 cm^{-1}, which has F2 g symmetry and can be viewed as a symmetric breathing mode of the O atoms around each cation. Since only the O atoms move, the vibrational mode is nearly independent of the cation mass [57,58]. The fast structural organization of CeO_2 particles processed in MAH can be related to the heating process which occurs from the interior to the surface. The microwave energy is transformed into heat through the interaction between molecules and atoms within the electromagnetic field. This interaction results in an internal and volumetric heating of the powders which promotes the formation of temperature gradients and heat flows.

Fig. 3 illustrates the UV–vis spectral dependence of absorbance for the ordered CeO_2 particles. The maximum absorption was located at around 400 nm with respective band gap values determined from the Kubelka Model [59]. The optical energy band gap is related to the absorbance and to the photon energy by the following Eq. (3):

$$h\nu\alpha \propto (h^{\circ} - E_g^{opt})^2 \quad (3)$$

where α is the absorbance, h is the Planck constant, ν is the frequency and E_g^{opt} is the optical band gap [60]. The band gap was deduced by fitting the absorption data to the direct transition equation by extrapolating the linear portions of the curves to absorption equal to zero. In structurally ordered CeO_2 particles, the absorbance measurements suggest a non-uniform band gap structure with a tail of localized states (see Fig. 3a–d). The decrease in the optical band gap energy [E(gap)] with the soaking time can be correlated to the reduction of structural defects or localized states inside the band gap which decreases the intermediary energy levels due to the reduction of oxygen vacancies located at crystal structure. The tendency observed shows that the optical band gap can be dependent on the preparation method and heat treatment. This behavior indicates that these samples present a certain structural order degree in agreement with the Raman spectra. The estimated band gaps were ranged between 2.65 and 2.97 eV. The uncertainty of these values was estimated at 0.05 eV. As soaking time increases, the optical band gap of the sample initially decreases and then increases because new levels of energy are formed promoting the appearance of intermediate electronic levels in the band gap. The irregularities in the optical band gap values can be related with the different preparation methods, shape, average crystal size and structural order–disorder degree in the lattice.

FEG-SEM micrographs of CeO_2 obtained at different soaking times are shown in Fig. 4. According to the image, most of the grains of CeO_2 powders are homogeneous with an average particle size calculated from the FE-SEM images of 6.7, 7.9, 8.8 and 11.5 nm at a soaking time of 1, 2, 4 and 8 min, respectively. CeO_2 powders obtained at lower soaking times display poor contrast and intense agglomeration amongst extremely fine particles. Aggregation between the particles decreases and monodispersed particles are observed at higher soaking times. The higher agglomeration degree of CeO_2 increased at lower soaking times due to Van der Waal's force derived for the –OH ligand precursor which was transformed to CeO_2 after hydrothermal treatment [60,61]. Moreover, the distribution in size seemed to be homogeneous and the shape appeared rounded. The synthesized ceria particles were relatively spherical with uniform size distribution, which was observed by FEG-SEM. Nanometric and isotropic CeO_2 crystallites obtained in this study are quite different from the previous study, where CeO_2 powders agglomerated into a cubic shape with the side size of 4.8 nm under hydrothermal conditions [62]. In the hydrothermal process, the presence of an alkaline medium was found to be essential.

The particle size of the CeO_2 powders was also examined using the TEM (Fig. 5). CeO_2 synthesized by MAH under KOH at 100 °C for 1, 2, 4 and 8 min, revealing the particle sizes

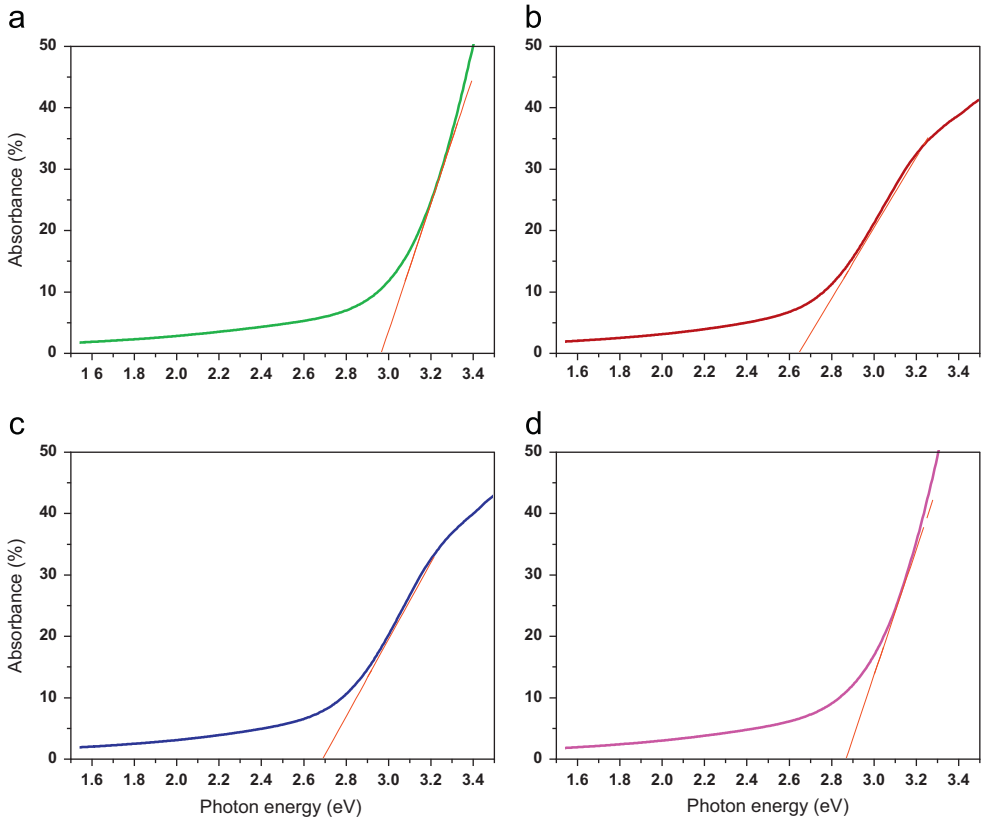

Fig. 3. UV–vis absorbance spectra of CeO_2 nanoparticles synthesized at 100 °C by the MAH method under different soaking times: (a) 1 min; (b) 2 min; (c) 4 min and (d) 8 min.

approximately range from 6 to 12 nm (Fig. 5a–d). The resultant particles have a spherical shape with a diameter of approximately 6 nm. However, Fig. 5d presents TEM micrographs of CeO_2 synthesized under MAH conditions on KOH mineralizer agent with a soaking time of 8 min. The particle size was higher (11 nm) with diameter of 4 nm and were homogeneously distributed compared to previous condition. The average particle size calculated from the TEM micrographs is 6.2, 7.4, 8.3 and 11.3 nm at a soaking time of 1, 2, 4 and 8 min, respectively. The small size of the CeO_2 particles synthesized at a lower soaking time can be explained quite simply. It is postulated that at the start of the reaction a large number of nuclei forms in the solution and as the reaction takes place in a very dilute solution there is not enough reactant left for the growth of the particles. As a result, the particles do not grow beyond 7 nm. After annealing at a higher soaking time, the large agglomerates disappeared and became smaller isometric ones and the maximum particle size decreased sharply attaining a value of 7 nm. There was not obvious change in the morphology under MAH conditions.

Fig. 6 shows the PL spectra of CeO_2 powders synthesized by MAH at 100 °C for 1, 2, 4 and 8 min under ambient condition according to the decomposition procedure of a band using a Gaussian response function and a Fourier decomposition/filtering algorithm. All the observations can be simply summarized. Whatever the sample be, band at 610 nm became more intense as particle size was reduced by hydrothermal treatment. As a consequence these bands may be attributed to bulk energy levels. This is consistent with their attribution to CT transitions between O^{2-} and Ce^{4+} [63]. A role of oxygen vacancies can be discarded as the samples are not doped. The band at 460 nm was shifted and became less intense with hydrothermal treatment: the effect was limited due to the particle size. The main difference between the samples under hydrothermal ripening was their crystal growth: very weak for a higher particle size and significant for a lower particle size. As a consequence this band may be attributed to surface specific defects that disappear during growth under hydrothermal conditions. It is noteworthy that these defects systematically exist in particles obtained by room temperature precipitation, whatever the pH, pressure and particle size are predominant. Interestingly, some cerium oxide particles directly synthesized in hydrothermal conditions did exhibit PL bands at 370 and 414 nm without significant emission at 460 nm [64], confirming that the intense peak at 460 nm was highly dependent on preparation processes. PL emission can be changed due to the presence of a large amount defects associated to the lower soaking time which affects the particle size. The PL is strongly dependent on the heat treatment conditions, showing that high soaking times cause a reduction in the defects or disorder of materials. Intensity of PL emission increases with the reduction of soaking time, as indicated in Fig. 6. This intensity is likely associated with structural disorganization level and the charge transfer occurring between cerium and oxygen ions. However, it is very important to note that at this condition no electronic levels of the amorphous $[CeO_4]$ clusters included in the wideband gap of the crystalline cluster were evidenced. This conclusion is a good indication that the PL of CeO_2 powders obtained by the MAH originates from intrinsic

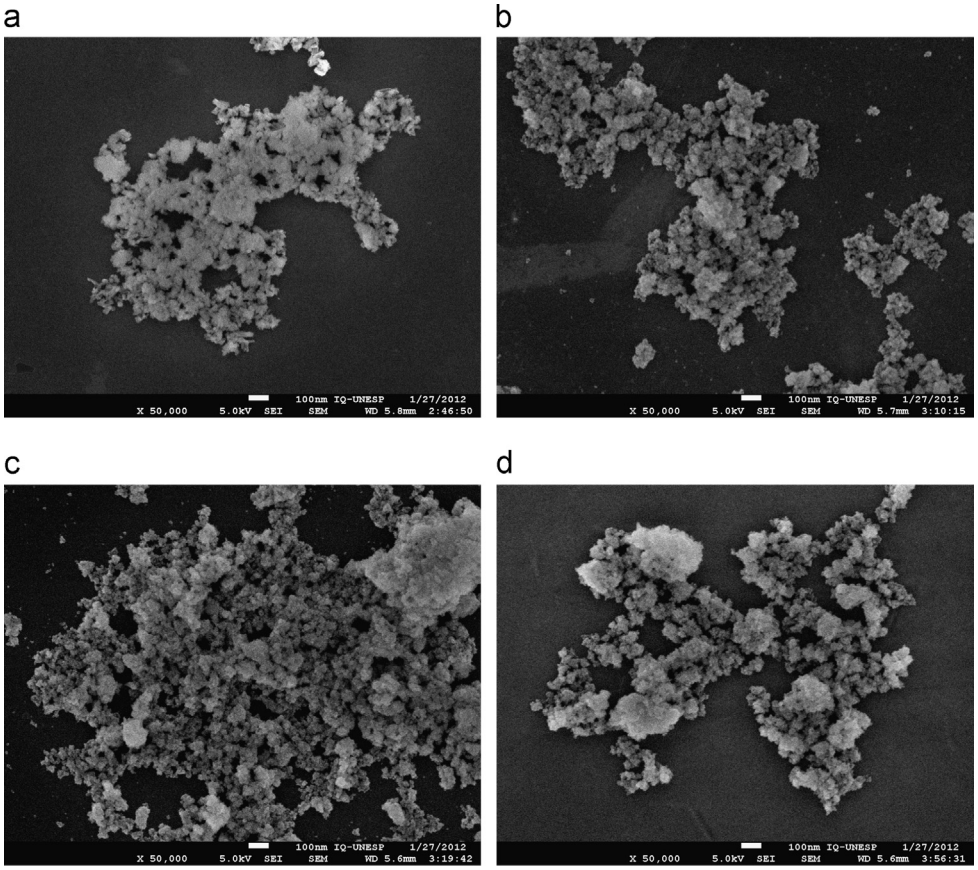

Fig. 4. FEG-SEM spectra of CeO_2 nanoparticles synthesized at 100 °C by the MAH method under different soaking times: (a) 1 min; (b) 2 min; (c) 4 min and (d) 8 min.

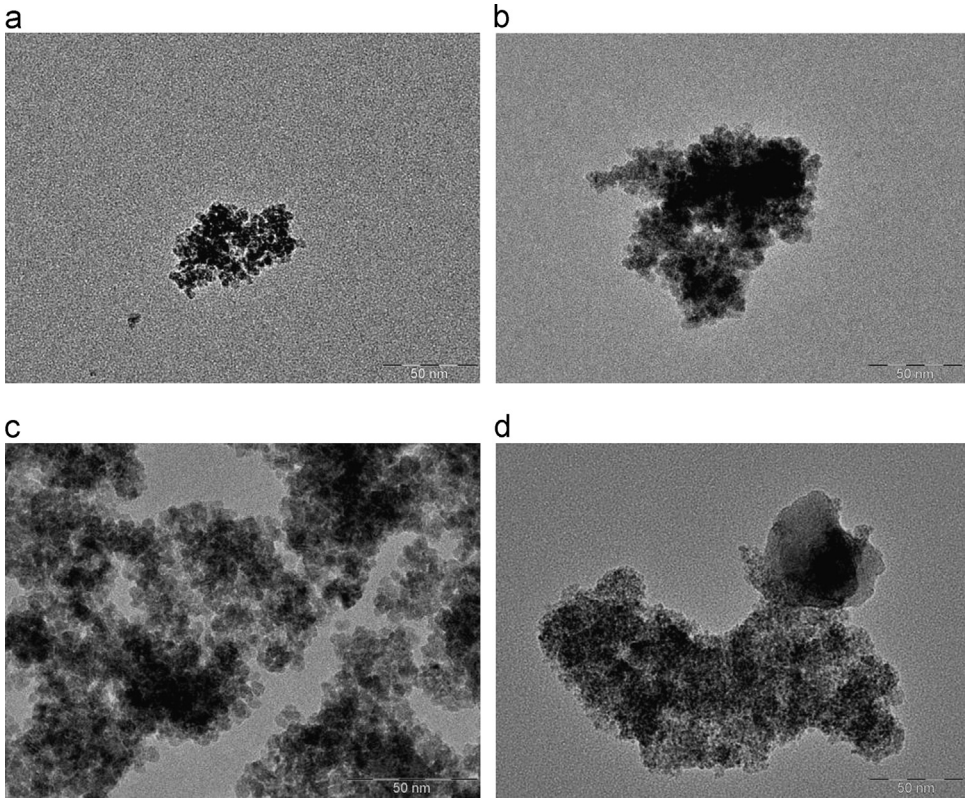

Fig. 5. TEM images of CeO_2 nanoparticles synthesized at 100 °C by the MAH method under different soaking times: (a) 1 min; (b) 2 min; (c) 4 min and (d) 8 min.

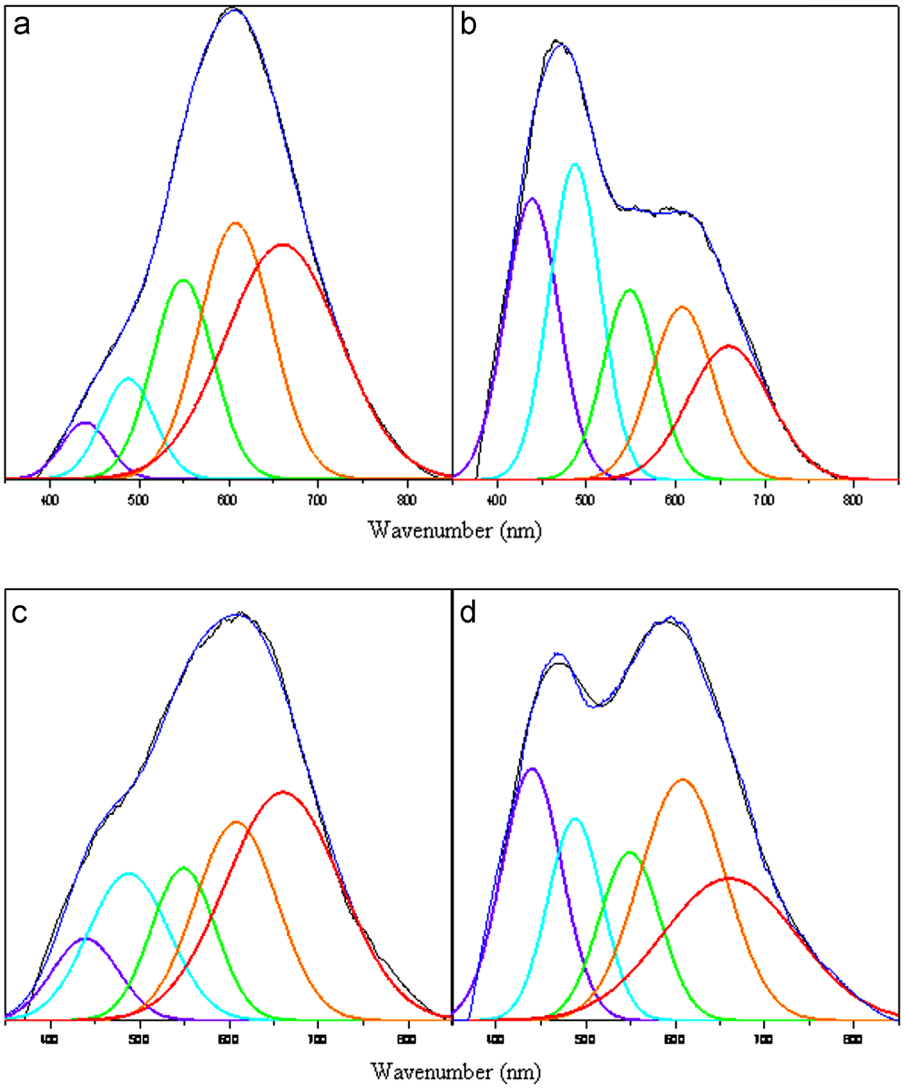

Fig. 6. PL spectra at room temperature of CeO_2 nanoparticles synthesized at 100 °C by the MAH method under different soaking times: (a) 1 min; (b) 2 min; (c) 4 min and (d) 8 min.

defects at lower soaking times and charge transfer after a certain degree of structural order.

4. Conclusions

Adopting the microwave-hydrothermal process as the synthesis method it is possible to obtain, by treating the solution at 100 °C for different soaking times, nanometric and crystalline ceria nanoparticles. The CeO_2 sample has better crystallization in the treatment at 8 min. FEG-SEM analysis has shown a homogeneous size distribution of nanometric CeO_2 crystallites. Raman scattering revealed the first scattering mode which is typical for cubic fluorite structure. CeO_2 synthesized by MAH under lower soaking times revealed agglomerate particles while CeO_2 synthesized under MAH conditions on higher soaking times were well-dispersed and homogeneously distributed. This can be explained by the amount of hydrogen bonds during the drying and calcining processes to form hard agglomerates of particles. UV–vis spectra revealed the presence of localized energy levels in the band gap of CeO_2 powders with a soaking time of 4 and 8 min possibly due to the certain structural order degree in the lattice. The PL emission intensity depends on different types of defects generated by a possible configuration arrangement interconversion in solution during CeO_2 growth under MAH conditions. The decrease in the band gap energy is associated to the localized levels in the band gap and with the charge discontinuities, which favors the trapping of electrons and holes to photoluminescent emission. MAH is important not only for the use of a short treatment time and low temperature but also for the possibility to control the morphological and structural properties. Therefore, the MAH method is undeniably a genuine technique for low temperatures and short times in comparison with the previous methodologies.

Acknowledgments

The financial support of this research project by the Brazilian research funding agencies CNPq and FAPESP is gratefully acknowledged.

References

[1] B.M. Reddy, A. Khan, Y. Yamada, T. Kobayashi, S. Loridant, J.C. Volta, Raman and X-ray photoelectron spectroscopy study of CeO_2–ZrO_2 and V_2O_5/CeO_2–ZrO_2 catalysts, Langmuir 19 (2003) 3025–3030.

[2] P. Bera, A. Gayen, M.S. Hegde, N.P. Lalla, L. Spadaro, F. Frusteri, F. Arena, Promoting effect of CeO_2 in combustion synthesized Pt/CeO_2 catalyst for CO oxidation, Journal of Physical Chemistry B 107 (2003) 6122–6130.

[3] G. Jacobs, L. Williams, U. Graham, D. Sparks, B.H. Davis, Low-temperature water-gas shift: In-situ DRIFTS—reaction study of a Pt/CeO_2 catalyst for fuel cell reformer applications, Journal of Physical Chemistry B 107 (2003) 10398–10404.

[4] R.X. Li, S. Yabe, M. Yamashita, S. Momose, S. Yoshida, S. Yin, T. Sato, Synthesis and UV-shielding properties of ZnO- and CaO-doped CeO_2 via soft solution chemical process, Solid State Ionics 151 (2002) 235–241.

[5] K. Sohlberg, S.T. Pantelides, S.J. Pennycook, Interactions of hydrogen with CeO_2, Journal of the American Chemical Society 123 (2001) 6609–6611.

[6] P. Jasinski, T. Suzuki, H.U. Anderson, Nanocrystalline undoped ceria oxygen sensor, Sensors and Actuators B—Chemical 95 (2003) 73–77.

[7] F. Goubin, X. Rocquefelte, M.H. Whangbo, Y. Montardi, R. Brec, S. Jobic, Experimental and theoretical characterization of the optical properties of CeO_2, $SrCeO_3$, and Sr_2CeO_4 containing Ce^{4+} (f(0)) ions, Chemistry of Materials 16 (2004) 662–669.

[8] D.G. Shchukin, R.A. Caruso, Template synthesis and photocatalytic properties of porous metal oxide spheres formed by nanoparticle infiltration, Chemistry of Materials 16 (2004) 2287–2292.

[9] B. Djuricic, S. Pickering, Nanostructured cerium oxide: preparation and properties of weakly-agglomerated powders, Journal of the European Ceramic Society 19 (1999) 1925–1934.

[10] S. Dikmen, P. Shuk, M. Greenblatt, H. Gocmez, Hydrothermal synthesis and properties of $Ce_{1-x}Gd_xO_2$-delta solid solutions, Solid State Sciences 4 (2002) 585–590.

[11] S.W. Zha, C.R. Xia, G.Y. Meng, Effect of Gd (Sm) doping on properties of ceria electrolyte for solid oxide fuel cells, Journal of Power Sources 115 (2003) 44–48.

[12] Y.R. Wang, T. Mori, J.G. Li, T. Ikegami, Low-temperature synthesis of praseodymium-doped ceria nanopowders, Journal of the American Ceramic Society 85 (2002) 3105–3107.

[13] J.G. Li, T. Ikegami, Y.R. Wang, T. Mori, 10-mol%-Gd_2O_3-doped CeO_2 solid solutions via carbonate coprecipitation: a comparative study, Journal of the American Ceramic Society 86 (2003) 915–921.

[14] M.J. Godinho, R.F. Goncalves, L.P.S. Santos, J.A. Varela, E. Longo, E.R. Leite, Room temperature co-precipitation of nanocrystalline CeO_2 and $Ce_{0.8}Gd_{0.2}O_{1.9}$-delta powder, Materials Letters 61 (2007) 1904–1907.

[15] R.A. Rocha, E.N.S. Muccillo, Preparation and characterization of $Ce_{0.8}Gd_{0.2}O_{1.9}$ solid electrolyte by polymeric precursor techniques, Advanced Powder Technology III 416 (2003) 711–717.

[16] S. Wang, K. Maeda, Direct formation of crystalline gadolinium-doped ceria powder via polymerized precursor solution, Journal of the American Ceramic Society 85 (2002) 1750–1752.

[17] F. Bondioli, A.B. Corradi, T. Manfredini, G. Leonelli, R. Bertoncello, Nonconventional synthesis of praseodymium-doped ceria by flux method, Chemistry of Materials 12 (2000) 324–330.

[18] H.Z. Song, H.B. Wang, S.W. Zha, D.K. Peng, G.Y. Meng, Aerosol-assisted MOCVD growth of Gd_2O_3-doped CeO_2 thin SOFC electrolyte film on anode substrate, Solid State Ionics 156 (2003) 249–254.

[19] H. Wang, J.J. Zhu, J.M. Zhu, X.H. Liao, S. Xu, T. Ding, H.Y. Chen, Preparation of nanocrystalline ceria particles by sonochemical and microwave assisted heating methods, Physical Chemistry Chemical Physics 4 (4) (2002) 3794–3799.

[20] H.M. Yang, C.H. Huang, A.D. Tang, X.C. Zhang, W.G. Yang, Microwave-assisted synthesis of ceria nanoparticles, Materials Research Bulletin 40 (2005) 1690–1695.

[21] M.M. Natile, G. Boccaletti, A. Glisenti, Properties and reactivity of nanostructured CeO_2 powders: comparison among two synthesis procedures, Chemistry of Materials 17 (2005) 6272–6286.

[22] J.S. Lee, S.C. Choi, Crystallization behavior of nano-ceria powders by hydrothermal synthesis using a mixture of H_2O_2 and NH_4OH, Materials Letters 58 (2004) 390–393.

[23] S. Komarneni, R. Roy, Q.H. Li, Microwave-hydrothermal synthesis of ceramic powders, Materials Research Bulletin 27 (1992) 1393–1405.

[24] S. Komarneni, Q. Li, K.M. Stefansson, R. Roy, Microwave-hydrothermal processing for synthesis of electroceramic powders, Journal of Materials Research 8 (1993) 3176–3183.

[25] S. Komarneni, Q.H. Li, R. Roy, Microwave-hydrothermal processing for synthesis of layered and network phosphates, Journal of Materials Chemistry 4 (1994) 1903–1906.

[26] S. Komarneni, R. Pidugu, Q.H. Li, R. Roy, Microwave-hydrothermal processing of metal powders, Journal of Materials Research 10 (1995) 1687–1692.

[27] F. Gao, Q. Lu, S. Komarneni, Fast synthesis of cerium oxide nanoparticles and nanorods, Journal of Nanoscience and Nanotechnology 6 (2006) 3812–3819.

[28] A.B. Corradi, F.B. Bondioli, A.M. Ferrari, T. Manfredini, Synthesis and characterization of nanosized ceria powders by microwave-hydrothermal method, Materials Research Bulletin 41 (2006) 38–44.

[29] T.N. Glasnov, C.O. Kappe, The microwave-to-flow paradigm: translating high-temperature batch microwave chemistry to scalable continuous-flow processes, Chemistry—A European Journal 17 (2011) 11956–11968.

[30] A. De la Hoz, A. Díaz-Ortiz, A. Moreno, Microwaves in organic synthesis. Thermal and non-thermal microwave effects, Chemical Society Reviews 34 (2005) 164–178.

[31] C.O. Kappe, Controlled microwave heating in modern organic synthesis, Angewandte Chemie International Edition 43 (2004) 6250–6284.

[32] T.L.C. Martins, T.C.C. França, C. Teodorico, T.C. Ramalho, J.D.F. Villar, Synthesis of guanylhydrazones under microwave irradiation, Synthetic Communications 34 (2004) 3891–3899.

[33] I. Bilecka, M. Kubli, E. Amstad, M. Niederberger, Simultaneous formation of ferrite nanocrystals and deposition of thin films via a microwave-assisted nonaqueous sol–gel process, Journal of Sol–Gel Science and Technology 57 (2011) 313–322.

[34] M. Estruga, C. Domingo, J.A. Ayllon, Microwave radiation as heating method in the synthesis of titanium dioxide nanoparticles from hexafluorotitanate-organic salts, Materials Research Bulletin 45 (2010) 1224–1229.

[35] V. Abdelsayed, A. Aljarash, M.S. El-Shall, Z.A. Al Othman, A.H. Alghamdi, Microwave synthesis of bimetallic nanoalloys and CO oxidation on ceria-supported nanoalloys, Chemistry of Materials 21 (2009) 2825–2834.

[36] M. Baghbanzadeh, S.D. Skapin, Z.C. Orel, C.O. Kappe, A critical assessment of the specific role of microwave irradiation in the synthesis of ZnO micro- and nanostructured materials, Chemistry—A European Journal 18 (2012) 5724–5731.

[37] S.-E. Park, Green catalysis by microwave synthesized nanostructured materials, Journal of Physics and Chemistry of Solids 69 (2008) 1501–1504.

[38] S. Saremi-Yarahmadi, B. Vaidhyanatha, K.G. Upul Wijayantha, Microwave-assisted low temperature fabrication of nanostructured α-Fe_2O_3 electrodes for solar-driven hydrogen generation, International Journal of Hydrogen Energy 35 (2010) 10155–10165.

[39] R.G. Deshmukh, S.S. Badadhe, I.S. Mulla, Microwave-assisted synthesis and humidity sensing of nanostructured α-Fe_2O_3, Materials Research Bulletin 44 (2009) 1179–1182.

[40] I. Bilecka, M. Niederberger, Microwave chemistry for inorganic nanomaterials synthesis, Nanoscale 2 (2010) 1358–1374.

[41] M. Baghbanzadeh, L. Carbone, P.D. Cozzoli, C.O. Kappe, Microwave-assisted synthesis of colloidal inorganic nanocrystals, Angewandte Chemie International Edition 50 (2011) 11312–11359.

[42] L.F. Silva, W. Waldir Avansi, M.L. Moreira, E. Longo, V.R. Mastelaro, Novel $SrTi_{1-x}Fe_xO_3$ nanocubes synthesized by microwave-assisted hydrothermal method, Cryst Eng Comm 14 (2012) 4068–4073.

[43] M.L. Moreira, A. Juan, V.R. Mastelaro, J.A. Varela, E. Longo, On the reversed crystal growth of $BaZrO_3$ decaoctahedron: shape evolution and mechanism, CrystEngComm 13 (2011) 5818–5824.

[44] L.R. Macario, M.L. Moreira, A. Juan, E. Longo, An efficient microwave-assisted hydrothermal synthesis of $BaZrO_3$ microcrystals: growth

mechanism and photoluminescence emissions, CrystEngComm 12 (2010) 3612–3619.
[45] D.-E. Zhang, X.-M. Ni, H.-G. Zheng, X.-J. Zhang, J.-M. Song, Fabrication of rod-like CeO_2: characterization, optical and electrochemical properties, Solid State Sciences 8 (2006) 1290–1293.
[46] S. Yu, H. Cölfen, A. Fischer, High quality CeO_2 nanocrystals stabilized by a double hydrophilic block copolymer, Colloids and Surfaces 243 (2004) 49–52.
[47] S. Maensiri, C. Masingboon, P. Laokul, W. Jareonboon, V. Promarak, P. Anderson, S. Seraphin, Egg white synthesis and photoluminescence of platelike clusters of CeO_2 nanoparticles, Crystal Growth and Design 7 (2007) 950–955.
[48] A. Morshed, M. Moussa, S. Bedair, R. Leonard, S. Liu, N. El-masry, Violet/blue emission from epitaxial cerium oxide films on silicon substrates, Applied Physics Letters 70 (1997) 1647–1649.
[49] F. Gao, G. Li, J. Zhang, F. Qin, Z. Yao, Z. Liu, Z. Wang, L. Lin, Growth and photoluminescence of epitaxial CeO_2 film on Si (111) substrate, Chinese Physics Letters 18 (2001) 443–444.
[50] D.-E. Zhang, X.-J. Zhang, X.-M. Ni, J.-M. Song, H.-G. Zheng, Fabrication of novel threefold shape CeO_2 dendrites: optical and electrochemical properties, Chemical Physics Letters 430 (2006) 326–329.
[51] B. Djuricic, S. Pickering, Silica-supported Au nanoparticles decorated by CeO_2: formation, morphology, and CO oxidation activity, Journal of the European Ceramic Society 19 (1999) 1925–1934.
[52] H.R. Tan, J.P.Y. Tan, C. Boothroyd, T.W. Hansen, Y.L. Foo, M.J. Lin, Experimental evidence for self-assembly of CeO_2 particles in solution: formation of single-crystalline porous CeO_2 nanocrystals, Journal of Physical Chemistry C 116 (2012) 242–247.
[53] H. Wang, J.J. Zhu, J.M. Zhu, X.H. Liao, S. Xu, T. Ding, Fabrication of porous metal oxides for catalytic applications using templating techniques, Physical Chemistry 4 (2002) 3794–3799.
[54] G.J. Wilson, A.S. Matijasevich, D.R.G. Mitchell, J.C. Schulz, G.D. Will, Modification of TiO_2 for enhanced surface properties: finite Ostwald ripening by a microwave hydrothermal process, Langmuir 22 (2006) 2016–2027.
[55] Y.W. Zhang, S. Rui, C.S. Liao, C.H. Yan, Fe doped CeO_2 nanoparticles, Journal of Physical Chemistry B 107 (2003) 10159–10163.
[56] M. Hirano, M. Inagaki, Preparation of monodispersed cerium (IV) oxide particles by thermal hydrolysis: influence of the presence of urea and Gd doping on their morphology and growth, Journal of Materials Chemistry 10 (2000) 473–477.
[57] J.R. McBride, K.C. Hass, B.D. Poindexter, W.H. Weber, Template preparation of nanoscale $Ce_xFe_{1-x}O_2$ solid solutions, Journal of Applied Physics 76 (1994) 2435–2441.
[58] P. Fornasiero, G. Balducci, R. DiMonte, J. Kaspar, V. Sergo, G. Gubitosa, Modification of the redox behaviour of CeO_2 induced by structural doping with ZrO_2, Journal of Catalysis 164 (1996) 83–173.
[59] M. Pineda, J.L.G. Fierro, J.M. Palacios, C. Cilleruelo, E. Garcia, J.V. Ibarra, Characterization of zincoxide and zinc ferrite doped with Ti or Cu as sorbents for hot gas desulphurization, Applied Surface Science 119 (1997) 1–10.
[60] P. Kubelka, F. Munk, Ein beitrag zur optik des farbanstriche, Zeitschrift für Technische Physik 12 (1931) 593–601 (in German).
[61] D.L. Wood, J. Tauc, Weak absorption tails in amorphous semiconductors, Physical Review B 5 (1972) 3144–3151.
[62] R. Lee Penn, J.F. Banfield, Imperfect oriented attachment: dislocation generation in defect-free nanocrystals, Science 281 (1998) 969–971.
[63] L. Li, H.K. Yang, B.K. Moon, Z. Fu, C. Guo, J.H. Jeong, S.S. Yi, K. Jang, H.S. Lee, Photoluminescence properties of CeO_2:Eu^{3+} nanoparticles synthesized by a sol–gel method, Journal of Physical Chemistry C 113 (2009) 610–617.
[64] C. Sun, H. Li, H. Zhang, Z. Wang, L. Chen, Controlled synthesis of CeO_2 nanorods by a solvothermal method, Nanotechnology 16 (2005) 1454–1463.